PERGAMON

International Journal of Multiphase Flow 26 (2000) 367–386

International Journal of Multiphase Flow

www.elsevier.com/locate/ijmulflow

Experimental study on transition of flow pattern and phase distribution in upward air–water two-phase flow along a large vertical pipe

Akira Ohnuki*, Hajime Akimoto

Japan Atomic Energy Research Institute, Tokai, Ibaraki 319-1195, Japan

Received 22 June 1998; received in revised form 23 March 1999

Abstract

In order to investigate the dependency of gas–liquid two-phase flow on pipe scale, the transition characteristics of flow pattern and phase distribution were studied experimentally in upward air–water two-phase flow along a large vertical pipe (inner diameter D: 0.2 m, the ratio of pipe length to diameter L/D: 61.5). The experiments were conducted under the flow rate: 0.03 m/s $\leq$ superficial air velocity (at top of test section) $\leq$ 4.7 m/s, 0.06 m/s $\leq$ superficial water velocity $J_L \leq 1.06$ m/s. Flow pattern was observed and measurements were performed on axial differential pressure, phase distribution, bubble size and bubble and water velocities. The scale effect was discussed with small-scale data (D: 0.025–0.038 m). The flow conditions at which coalescence starts are almost the same as those found in small-scale pipes, but no large bubbles are observed in the region $L/D < 20$ which corresponds to the developing region of the axial differential pressure curves. The large coalescent bubbles were generated in $L/D > 20$. The churn flow is dominant in the large vertical pipe under the conditions where small-scale pipes have slug flow. The transition of phase distribution corresponds to the change of flow pattern. Large coalescent bubbles affect the phase distribution as similar to small-scale pipes but the following remarks are concluded as the scale effect: (1) under a low J_L where small-scale pipes have a wall-peak phase distribution, a core-peak phase distribution is established, where some large eddies including bubble clusters fill up the pipe, (2) the large coalescent bubbles are developed along the test section via the churn bubbly flow where the phase distribution is a core peak one, whereas Taylor bubbles in small-scale pipes are generated at the vicinity of gas–liquid mixing region or are developed from the bubbly flow with a wall-peak phase distribution, (3) the wall-peak in the large vertical pipe is lower even under

* Corresponding author.
E-mail address: ohnuki@hflwing.tokai.jaeri.go.jp (A. Ohnuki).

PII: S0301-9322(99)00024-5

the same bubble size. The lower peak is considered to be related to the lower radial velocity gradient of water and the larger turbulent dispersion force.

Keywords: Gas–liquid two-phase flow; Large diameter; Vertical pipe; Flow pattern; Bubbly flow; Churn flow; Phase distribution; Bubble diameter; Scale effect; Lift force; Turbulent dispersion force

1. Introduction

To resolve flow mechanism for establishing a phase distribution is recognized to be one of important subjects on investigating a fine structure under gas–liquid two-phase flow (Serizawa and Kataoka, 1988). The shape of phase distribution has been reported to depend on the bubble diameter by several experimental works (Bataille et al., 1990). A numerical simulation using an interface-tracking method (Tomiyama et al., 1995) also confirmed the finding. However, it is not clear whether physical models based on the finding with the small-scale experiments and the simulation under laminar condition can also apply to the prediction of two-phase flow in a large diameter pipe, which is important in many industrial applications. To make clear the scale problems, database with detailed measurements against a large diameter pipe is indispensable but such database is scarce.

In order to establish the database, we performed air–water experiments with a large vertical pipe (Ohnuki et al., 1995; Ohnuki and Akimoto, 1996; Ohnuki et al., 1997). We used two test sections: one is inner diameter D of 0.48 m and ratio of length L to D of about 4.2 (small L/D geometry) and another is D of 0.2 m and L/D of about 60 (large L/D geometry). In the experiments, the flow pattern and the phase distribution near the top of test section were investigated and the following conclusions were obtained:

1. The flow conditions at the start of coalescence in the large L/D geometry are almost the same as those in narrower pipes, but where the narrow pipes have slug flow, churn flow is found in the wider pipe. No slug bubbles, which occupied the pipe cross-section, were

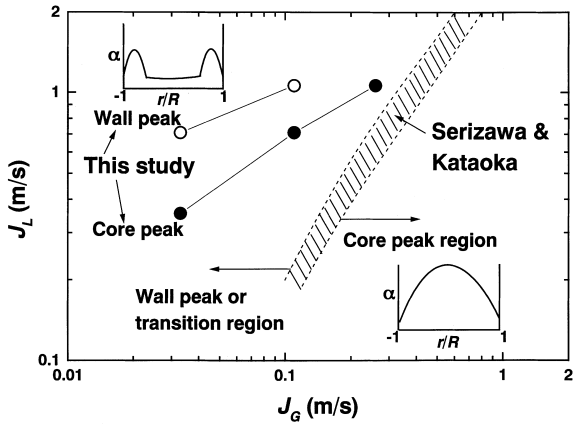

Fig. 1. Comparison of transition boundary in J_G–J_L map from wall-peak to core-peak regions of phase distribution.

recognized in the small L/D geometry.

2. The phase distribution near the top of the large L/D geometry was classified into a wall-peak phase distribution or a core peak one depending on the flow rate. The boundary between the phase distributions locates under lower superficial air velocity (J_G) and higher superficial water velocity (J_L) than for small-scale pipes by Serizawa and Kataoka (1988), as shown in Fig. 1 (α: void fraction, r: radial position from pipe center, R: radius of pipe). The results in Fig. 1 indicate that the boundary is difficult to be correlated with only the relation of J_G and J_L for wide variety of the pipe scale.

For small-scale pipes, many experimental studies have been reported on the relationship between the flow rate and the phase distribution (Serizawa and Kataoka, 1988). Using the database, several sets of constitutive equations for two-fluid model have been recommended to predict a wall-peak phase distribution (Anglart et al., 1993; Bertodano et al., 1994a,b; Minato et al., 1996). Our studies, mentioned above, give similar database for the large vertical pipe. However, to understand the scale effect, e.g., the discrepancy shown in Fig. 1, more detailed measurements are needed, such as bubble size and velocity distribution including the transition along the pipe which were not measured in our previous studies. This is because a lateral lift force affecting the phase distribution depends on the bubble size and the velocity gradient (Anglart et al., 1993; Tomiyama et al., 1995).

For large vertical pipes, there are several previous studies by other researchers but most of the works are related to flow pattern and one-dimensional analyses. Kataoka and Ishii (1987) summarized previous studies (D: 0.011–0.61 m, fluid: air–water, air–glycerin and steam–water, pressure: 0.101–18.2 MPa) and developed a new drift-flux type correlation for pool void fraction. Under bulk liquid flow condition in air–water two-phase flow, Hills (1976) proposed a correlation for average void fraction in a vertical pipe with D of 0.15 m (L/D: 70). Hashemi et al. (1986) investigated the flow pattern and void fraction in a specific geometry with D of 0.1 m (L/D: 30) or 0.3 m (9.5), the geometry which simulated once-through steam generators of Babcock and Wilcox (B and W) pressurized water reactor, i.e., a horizontal inlet pipe connected to a vertical pipe via an elbow with a bend at the vertical pipe exit. From these studies, the database for the average void fraction is supposed to be enough, although effects of the bulk liquid flow have not been investigated in steam–water system. However, studies on flow structure (phase and velocity distributions) including the flow pattern scarcely exist.

In this study, we investigate experimentally the transition characteristics of flow pattern and phase distribution in upward air–water two-phase flow along a large vertical pipe to examine the dependency on the pipe scale. The transition will be studied under a wide range of flow rate including the transition along the axial direction using the large L/D geometry. Various measurements such as bubble size, water velocity and bubble velocity are also performed. The databases by Leung et al. (1995) (D: 0.0254 m, L/D at measuring locations: 12, 62, 112) and Liu and Bankoff (1993a,b) (0.038 m, 36) are used in the discussion of the scale effect.

2. Experiment

The experimental rig used in this study is almost the same as that in the previous study

(Ohnuki et al., 1997), except for an air injection device. Local void fraction was measured under a wider range of flow rate than that in the previous study. The physical quantities for air bubbles (e.g., bubble size, bubble velocity and velocity fluctuation) and water (e.g., water velocity and velocity fluctuation) were newly obtained in this study. The axial distribution of differential pressure was also measured in this study.

Fig. 2 shows the outline of the experimental rig. The experimental rig is composed of a test section, an upper plenum located above the test section, a lower plenum below the test section and the air and water sources. The test section is made of a transparent acrylic resin to observe the flow pattern. D and L of the test section are 0.2 and 12.3 m, respectively. The upper and the lower plena are made of stainless steel and the dimensions are inner diameter: 1 m and height: about 1 m. The lower plenum can set up the air injection device inside the plenum, which uses a porous sinter tube (grain size: 40 μm). The detail of the device is shown in Fig. 3. The device consists of four units, and each unit has three sinter tubes on a base whose cross-section is a rectangular shape. Air flow rate to each unit can be adjusted independently.

The air was fed from compressors via an orifice flow meter to the air injection device. The water was injected into the bottom of the lower plenum via an electromagnetic flow meter. The water temperature was kept to be constant, about 30°C, by a cooler to remove heat from a pump. The top of the upper plenum is open to the atmosphere.

The measurement items and a specification of each item are listed in Table 1. The flow pattern and the sectional differential pressure along axial direction were recorded under the whole range of flow rate in this study. The local void fraction was measured under relatively

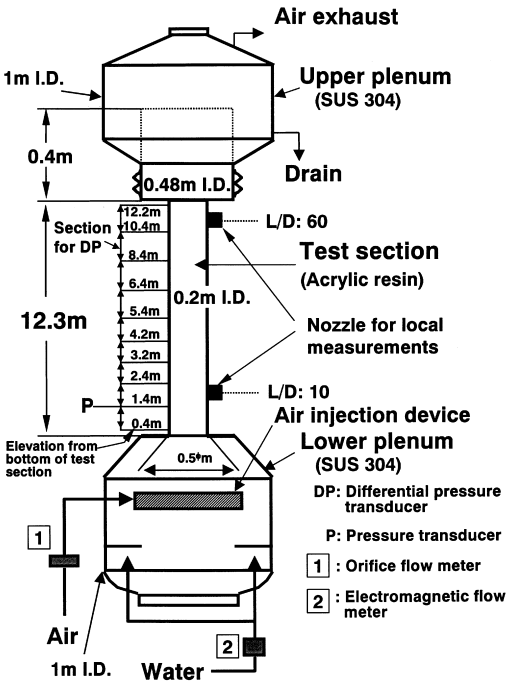

Fig. 2. Schematic of experimental rig.

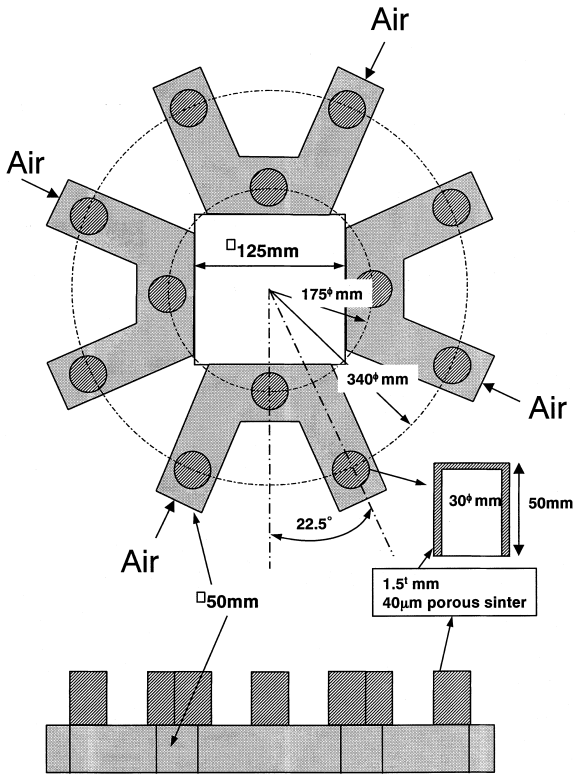

Fig. 3. Schematic of air injection device.

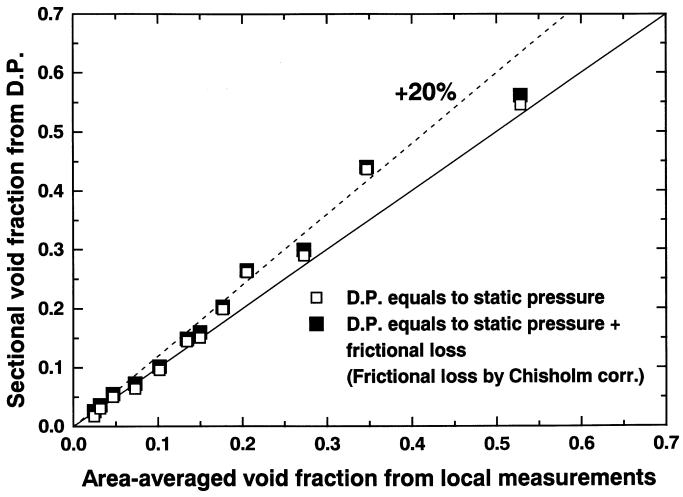

Fig. 4. Evaluation of uncertainty for local void fraction measurements.

Table 1
List of measurement items and specification of each item in this study

Item	Method	Sampling rate	Measuring time	Accuracy etc.	Flow rate condition (at top of test section)
Flow pattern	Visual observation; still picture	–	–	–	J_G: 0.03–4.7 m/s; J_L: 0.06–1.06 m/s
Differential pressure	Differential pressure transducer	20 Hz	100 s	$\pm$ 0.2 kPa/m (Max)	J_G: 0.03–4.7 m/s; J_L:0.06–1.06 m/s
Void fraction	Optical void probe (KANOMAX JAPAN (Ltd.) System 7933)	10 kHz	300 s	Sensor tip diameter: 0.35 mm, minimum time passing a bubble: 0.6 ms, see Fig. 4	J_G: 0.03–3.1 m/s; J_L: 0.18–1.06 m/s
Bubble velocity and velocity fluctuation	Dual-sensor resistivity probe (Custom-made sensor + KANOMAX JAPAN (Ltd.) System 7931)	10 kHz	12.5 s	Sensor tip diameter: 0.1 mm, axial distance between two tips: 2.92 mm, minimum time passing a bubble: 0.3 ms	J_G: 0.03, 0.11, 0.26 m/s; J_L: 1.06 m/s
Bubble diameter	DC output from optical void probe + bubble velocity	10 kHz	12.5 s	–	J_G: 0.03, 0.11, 0.26 m/s; J_L: 1.06 m/s
Water velocity and velocity fluctuation	X-type hot film anemometer (KANOMAX JAPAN (Ltd.) Sensor Model 1246-60 W, System 7114)	50 kHz	10 s	Sensor diameter: 0.15 mm, length: 2 mm	J_G: 0.0, 0.03, 0.11 m/s; J_L: 1.06 m/s

wide range of flow rate, but the other quantities were obtained under specified conditions around the transition region of phase distribution shown in Fig. 1.

The local time-averaged void fraction was measured by the optical void probe in Table 1. The accuracy of the local measurements was evaluated by the sectional differential pressure measurements and the results are shown in Fig. 4. The void fraction from the local measurements was obtained by the integration over the plane at the measurement elevation. The integrated error is less than about 20%. The sectional void fraction from differential pressure (DP) was estimated under the assumption that the DP equals to static pressure or that the DP equals to static pressure plus frictional loss. The Chisholm–Laird correlation was used for the evaluation of frictional pressure loss. The effect of the frictional loss is small as shown in Fig. 4.

The bubble size at a radial position was derived with the time-series data by the optical probe and with bubble velocity measurements by the dual-sensor resistivity probe in Table 1. The design of the dual-sensor resistivity probe is similar to that in the study by Liu and Bankoff (1993b). Since the data by Liu and Bankoff are intended to be used as the main database for small-scale pipes in this study, their methodology for estimating the bubble velocity and the bubble diameter is adopted to minimize an additional difference in analysing the scale effect in Section 3.3.

The local time-averaged bubble velocity in the axial direction $U_G(r)$ can be determined if the bubble mean transport time, $t_0(r)$, and the axial distance between tips of the dual-sensor, d, are known. Thus

$$U_G(r) = \frac{d}{t_0(r)} \tag{1}$$

Both multichannel analysis and the cross-correlation method were used to determine t_0. The former method gives the spectrum of the time lag for each bubble, while the latter gives the most probable time lag between the two sensor output signals. Based on the former method, the local bubble velocity $U_G(r)$ and its axial turbulent fluctuation $u'_G(r)$ are determined by

$$U_G(r) = \frac{\sum_i N_i U_{Gi}(r)}{\sum_i N_i} \tag{2}$$

$$u'_G(r) = \left\{ \frac{\sum_i N_i \left[U_{Gi}(r) - U_G(r) \right]^2}{\sum_i N_i} \right\}^{1/2} \tag{3}$$

where U_{Gi} is the instantaneous measured local bubble velocity in ith channel, and N_i is the counting rate in each channel of U_{Gi}. The bubble velocity $U_G(r)$ by this method was very close to the one obtained from the cross-correlation method. The accuracy of the bubble velocity

measurements was checked with J_G by integrating the product of local void fraction α and $U_G(r)$. The integrated values were within the error of $\pm 5\%$.

The bubble diameter was derived based on the concept that the bubble size distribution is related to the probability density function of bubble chord length. The following equation was used in the derivation:

$$d_{av}(r) = 1.5 \int_0^\infty x g(x)\, dx \tag{4}$$

where $d_{av}(r)$ is the local average bubble diameter, x is the axial bubble chord length and $g(x)$ is the probability density function of bubble chord length. This method is the same as that in the study by Liu and Bankoff, and the bubble is assumed to be the spherical shape. We know that the spherical assumption brings a considerable difference from reality for bubbles with a larger size more than about 4 mm (equivalent spherical diameter, air–water system) (Zun et al., 1995). But, we nonetheless adopt Eq. (4) because the scale effect will be discussed with the database by Liu and Bankoff where the bubble size is estimated by Eq. (4).

In this study, the bubble chord length was estimated using time-averaged bubble velocity. This method has a tendency to underestimate the length of larger bubbles because larger bubbles rose faster. As listed in Table 1, the length was derived under J_G: 0.03, 0.11, 0.26 m/s and J_L: 1.06 m/s in this study. We observed coalescent larger bubbles under $J_G = 0.26$ m/s.

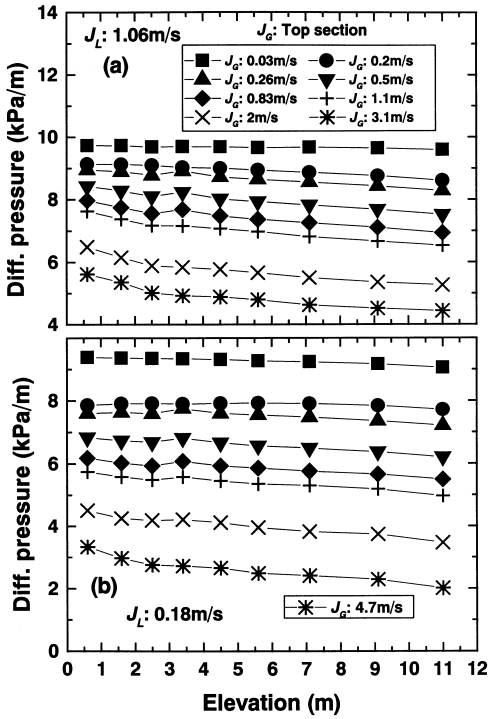

Fig. 5. Axial distribution of sectional differential pressure: (a) high J_L condition and (b) low J_L condition.

Although the number density of larger bubbles was low under the condition, we should pay attention to use carefully the length of larger bubbles in quantitative discussions.

The local time-averaged water velocity in the axial direction $U_L(r)$ was measured by the dual-sensor X-type hot-film probe (KANOMAX JAPAN (Ltd.) 1246-60W), which is almost the same one used in the study by Liu and Bankoff (1993a). Their methodology for estimating the water velocity is also adopted in this study. The axial turbulent fluctuation $u'_L(r)$ was derived by the signal of the probe with the same methodology by Liu and Bankoff. The accuracy of the water velocity measurements was checked with J_L by integrating the product of $1-\alpha$ and $U_L(r)$. The integrated values were within the error of $\pm 5\%$.

3. Results and discussion

3.1. Differential pressure and flow pattern

Fig. 5 compares the axial distribution of sectional differential pressure under various flow rates. J_G was estimated using the pressure at top of test section. The differential pressure decreases with increasing J_G and with elevation because the void fraction increases with J_G and the increase of frictional pressure loss is not significant. Almost linear relationship between the

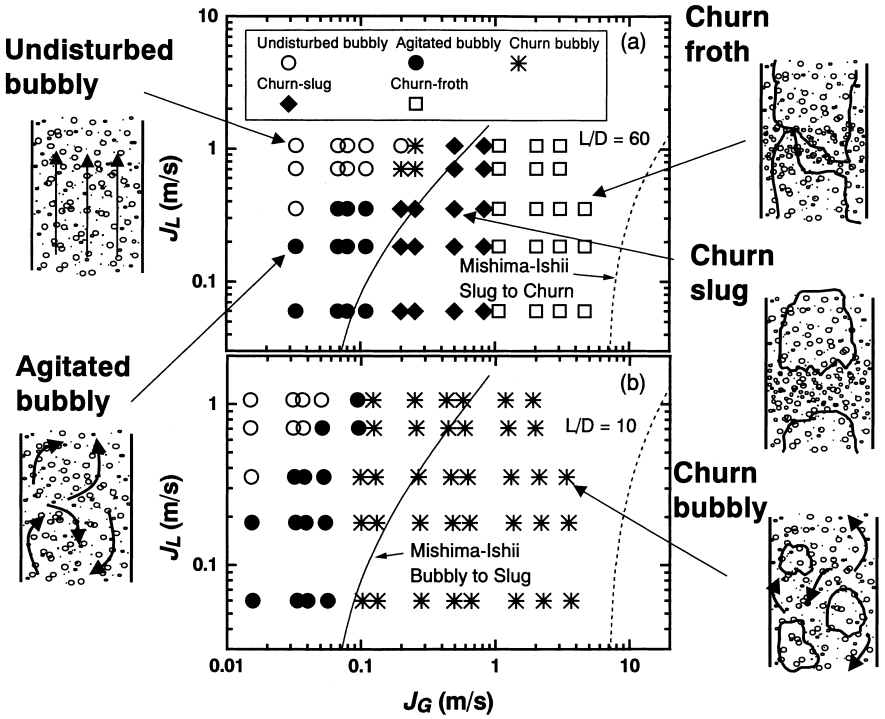

Fig. 6. Transition of flow pattern: (a) top region of test section; $L/D = 60$ and (b) bottom region of test section; $L/D = 10$.

differential pressure and the elevation is attained under a low J_G (0.03 and 0.2 m/s) and in the region above, about 4 m, under the higher J_G. The linear relationship at each flow rate indicates that no significant flow acceleration and/or deceleration is existed and the change of two-phase flow along the elevation is realized mainly due to the static pressure change. But the relationship in the region below, about 4 m, under the higher J_G shows a curved line or a different gradient with elevation against that above 4 m. These different characteristics are considered to be affected by a developing flow, which is characterized as a non-equilibrium flow where the flow significantly accelerates and/or decelerates with bubble coalescence/disintegration. In this study, the observation of flow pattern and the local measurements for phase distribution, bubble velocity etc. were performed at $L/D = 10$ and 60. We should recognize that the developing flow affects the physical quantities at $L/D = 10$.

The flow pattern was basically changed from a bubbly flow to a churn froth flow with J_G at a fixed J_L, but no large coalescent bubbles like slug bubbles were observed near the bottom region of the test section even under a higher J_G. Fig. 6 indicates the flow pattern map near the top region (a) and the bottom region (b) of the test section. The boundary between bubbly and slug flows and that from slug to churn flows by Mishima and Ishii (1984) are included in this map. For the top region, an undisturbed or an agitated bubbly flow is realized in the bubbly flow region of the Mishima–Ishii map. And in the slug flow region of the Mishima–Ishii map, large coalescent bubbles are existed and the flow pattern is changed to a churn froth flow via a churn bubbly and/or a churn slug flow with J_G. The transition condition of J_G to the churn flow is lower than that of the Mishima–Ishii map. The bubble coalescence predominated at a certain elevation. Below the elevation, the flow pattern was characterized as the churn bubbly flow under the higher J_G, where a developing process with bubble coalescence/disintegration was occurred. The elevation, where large coalescent bubbles start to flow upwards, was in the region of 3–4 m. This elevation corresponds to the transition of the differential pressure characteristics at about 4 m in Fig. 5.

The following remarks are clearly stated to be different from small-scale pipes (Mishima and Ishii, 1984; Dukler and Taitel, 1986):

1. Under a lower J_L in the bubbly flow region, the agitated bubbly flow is observed, where the bubbly flow pattern was agitated due to random movement of bubble clusters. In the agitated bubbly flow, some large eddies including bubble clusters fill up the pipe. The flow direction of a cluster was random due to the large eddy and some bubble clusters with downward flow direction were frequently observed.
2. In the churn slug/froth flow region, large coalescent bubbles flow intermittently as similar to the slug flow in a small-scale pipe but there are many small bubbles in the liquid film region between the large bubble and the wall.

The flow patterns of the undisturbed bubbly flow and the agitated one are similar to those in the previous study (Ohnuki et al., 1995) using the small L/D geometry (D of 0.48 m and L/D of about 4.2). Both flow patterns in the small L/D geometry were also observed under the bubbly flow condition of the Mishima–Ishii map, and the boundary between the undisturbed bubbly flow and the agitated one in the J_G–J_L map was located near that, in this study. But in the previous study, there were no large coalescent bubbles occupying the pipe under the slug flow region of the Mishima–Ishii map, where an unstable and oscillatory behaviours of bubble

clusters were observed. Since the similar flow pattern is observed near the bottom region of the present test section, the flow pattern in the slug flow region is considered to be strongly affected by L/D and the coalescence of bubbles changes the flow pattern in a large L/D geometry.

3.2. Phase distribution

Figs. 7 and 8 show the variation of phase distribution on the effect of J_G and of J_L near the top of test section, respectively. The phase distribution in this large vertical pipe is also classified into the wall-peak phase distribution or the core peak one depending on the flow rate as for small-scale pipes (Serizawa and Kataoka, 1988). The difference between the local void fraction at the wall-peak region and at the core region tends to be smaller with increasing J_G or decreasing J_L and the radial shape changes to the convex shape. The shape of phase distribution is almost maintained as a symmetrical one on the pipe center. The flow rate conditions on the shape transition correspond to the map of Fig. 1 (J_G from 0.11 to 0.26 m/s in Fig. 7 and J_L from 0.71 to 1.06 m/s in Fig. 8). The transition conditions also correspond to the transition of flow pattern, i.e., from the undisturbed bubbly to the churn bubbly or the agitated bubbly flow. In the churn bubbly flow, bubble coalescence/disintegration processes became significant, and a wider spectrum of bubble size can be supposed. In fact, the spectrum was wider than the undisturbed bubbly flow as shown below. Since the lateral lift force was

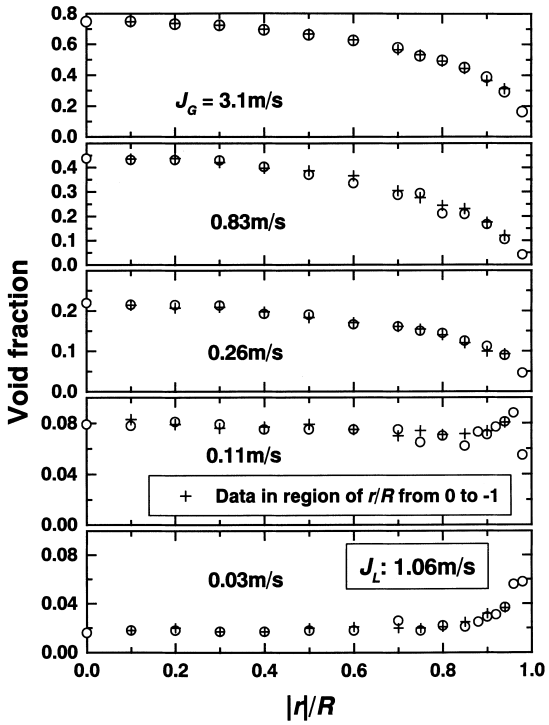

Fig. 7. Effect of air velocity on phase distribution near top of test section ($L/D = 60$).

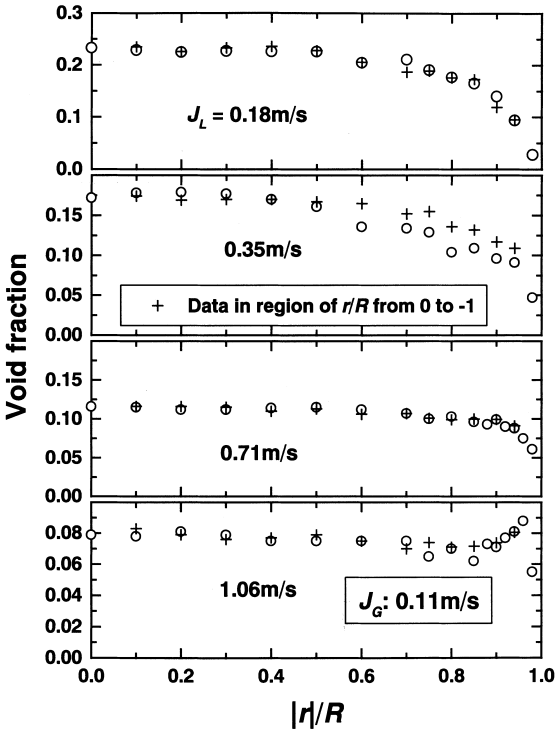

Fig. 8. Effect of water velocity on phase distribution near top of test section ($L/D = 60$).

reported to be affected by the bubble size (Tomiyama et al., 1995), the wider spectrum of bubble size is supposed to affect the transition of phase distribution as for small-scale pipes (Serizawa and Kataoka, 1988; Zun et al., 1993).

Fig. 9 compares several quantities near the transition conditions from the wall-peak to the core-peak phase distributions at the top region. And the spectrum of the probability density function of bubble chord length $g(x)$ in Eq. (4), at pipe center, is compared in Fig. 10. Since large coalescent bubbles were sometimes observed under the churn bubbly flow, the average bubble diameter in $|r|/R$ less than about 0.8 is larger, and the bubble velocity and its fluctuation are higher under the higher J_G condition. The bubble chord length spectrum also indicates that several larger bubbles are realized under the churn bubbly flow. These results support that the formation of large bubbles affects the phase distribution also for the large vertical pipe.

The variation of phase distribution along the pipe was examined under churn bubbly and churn slug flows. Fig. 11 compares the phase distribution including bubble size and bubble velocity between the top ($L/D = 60$) and the bottom ($L/D = 10$) regions under the churn bubbly flow. The spectrum of $g(x)$ in Eq. (4), at pipe center, is also compared in Fig. 12. The local void fraction at the bottom region is lower than that at the top region. As for the shape of phase distribution, the convex shape and the symmetrical one on the pipe center are maintained even at the bottom region. Although the shape of phase distribution is similar, a flow development along the pipe is recognized on the bubble diameter and its related

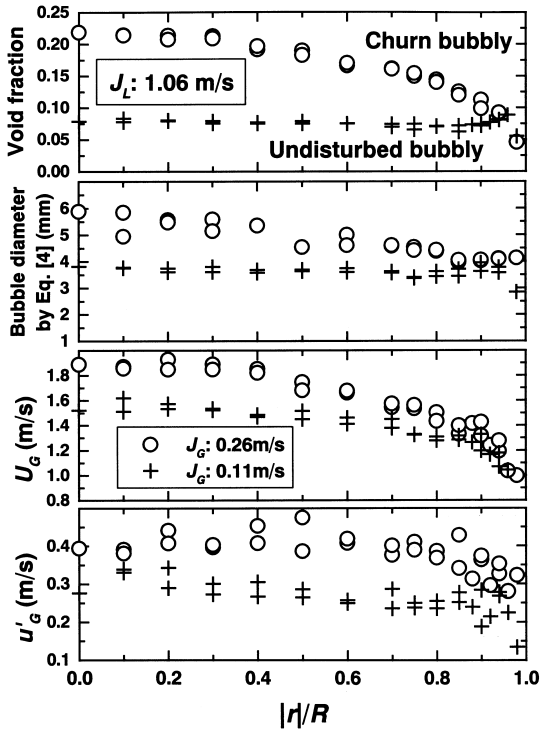

Fig. 9. Comparison of phase distribution, bubble diameter by Eq. (4), axial bubble velocity and velocity fluctuation near the transition flow conditions from wall-peak to core-peak phase distributions.

quantities. The average bubble size is slightly smaller in $|r|/R$ less than about 0.4 and the bubble velocity is lower at the bottom region. The bubble chord length more than 40 mm is appeared at the top region but the length at the bottom region is less than about 30 mm. These differences are considered to be caused by a developing process of bubble coalescence/

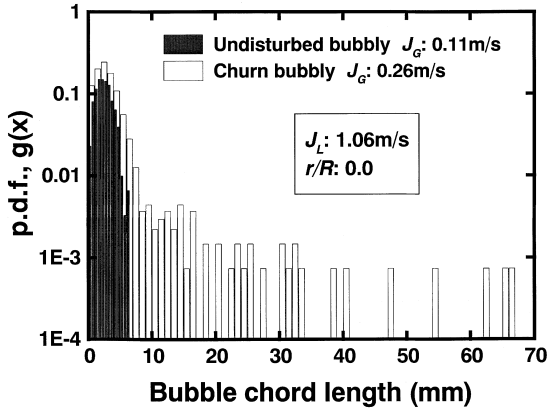

Fig. 10. Comparison of probability density function of bubble chord length near the transition flow conditions from wall-peak to core-peak phase distributions.

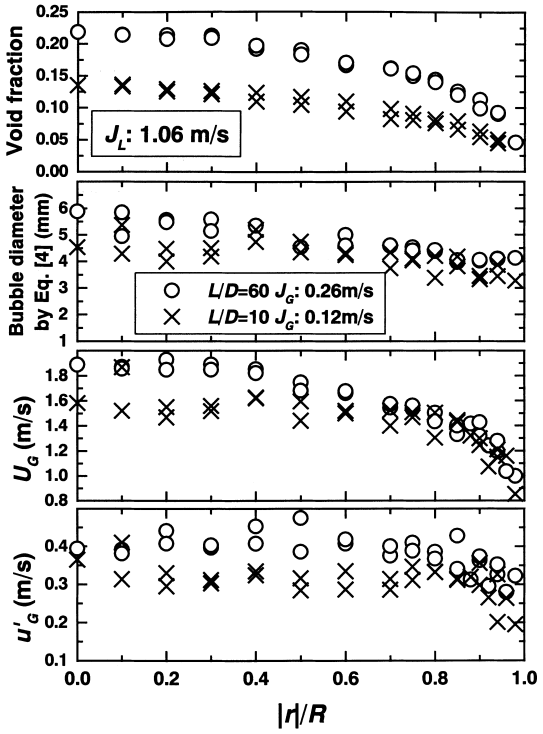

Fig. 11. Comparison of phase distribution, bubble diameter by Eq. (4), axial bubble velocity and velocity fluctuation between at bottom and top regions of test section.

disintegration. The effect of a developing flow is recognized also on the differential pressure in Fig. 5 under this condition. The bubble size and its related quantities can be important measures to investigate the developing process of two-phase flow.

J_G condition at the bottom region in Fig. 11 is almost the same as that under the undisturbed bubbly flow in Fig. 9, and the area-averaged void fraction is almost the same each

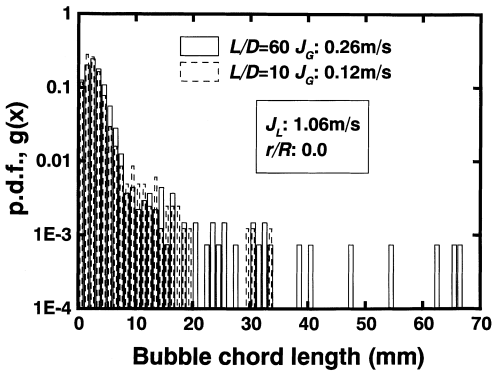

Fig. 12. Comparison of probability density function of bubble chord length between at bottom and top regions of test section.

other. However, the phase distribution is totally different. This difference is considered to be related to the difference of bubble size. The time-averaged bubble size is almost the same between the conditions as shown in Figs. 9 and 11 but the spectrum is wider under $L/D = 10$ as compared Fig. 12 with Fig. 10. Zun et al. (1993) reported in a small-scale rectangular pipe that the wall to core-peak transition was realized in terms of the difference of bubble size even under the same area-averaged void fraction. In their study, the phase distribution changed to a core peak one under the bubble equivalent spherical diameter more than 5.8 mm. The phase distribution is not necessarily classified only by the flow rate and local physical quantities such as the bubble size and its spectrum should be carefully investigated also for the large vertical pipe.

3.3. Scale effect on phase distribution

In the previous sections, the transition of flow pattern and phase distribution under a wide range of flow rate were examined including the transition along the axial direction. In this section, we focus on the scale effect of pipe on the phase distribution. The axial transition is compared with the database by Leung et al. (1995), and the different characteristics under the wall-peak phase distribution are discussed using Liu and Bankoff (1993a,b) database. Through this investigation, we expect to clarify the different flow structure in the large-scale pipe from that in a small-scale one.

Fig. 13 compares the axial transition under churn bubbly/slug flows in this study with bubbly to slug flows in (Leung et al., 1995). The flow conditions in this figure are near the flow

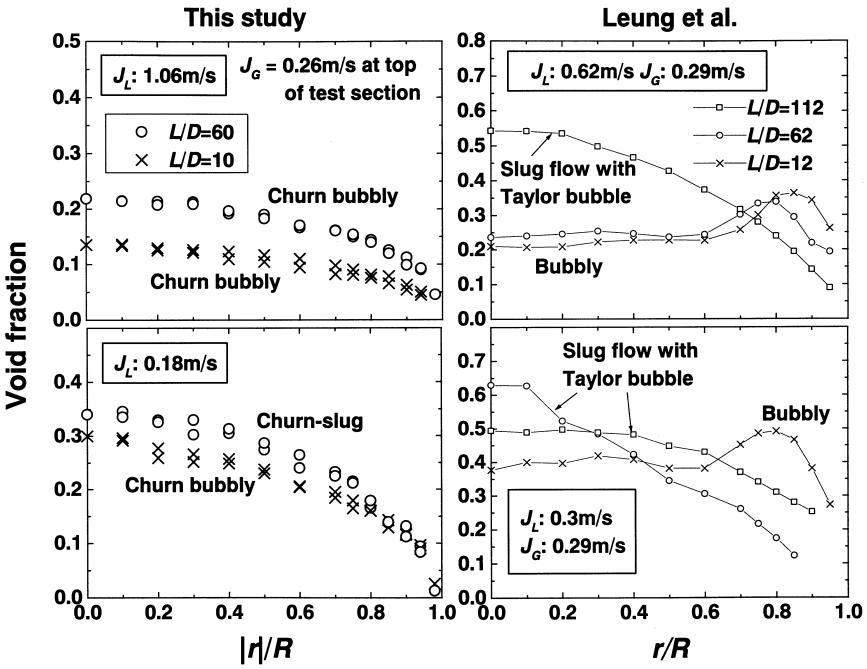

Fig. 13. Comparison of phase distribution along test section with small-scale data.

pattern transition in each pipe where the development of large bubbles begins. In the large vertical pipe, the large coalescent bubbles were developed along the test section via the churn bubbly flow, and the shape of phase distribution was not changed between the bottom and the top regions as shown in this figure. These characteristics on the formation of large bubbles and the shape of phase distribution were observed under the churn bubbly/slug flows and the churn froth flow in this study. In contrast, the shape change is attained along the small-scale pipe. In the small-scale pipe, Taylor bubbles were generated at the vicinity of gas–liquid mixing region or were developed from the bubbly flow with a wall-peak as shown in this figure (Leung et al., 1995). The wall-peak in the large vertical pipe was realized only under the undisturbed bubbly flow where no bubble coalescent processes were observed and the area-averaged void fraction was low. Although it is not clear the flow development under $L/D > 60$, the formation of large bubbles from the undisturbed bubbly flow is considered to be difficult in the large vertical pipe.

As revealed in the previous sections, the bubble size is one of important quantities to govern the phase distribution. Thus, the flow structure under the wall-peak phase distribution is examined under almost the same bubble size. Fig. 14 compares the phase distribution and the bubble diameter by Eq. (4) between this study at $L/D = 60$ and in (Liu and Bankoff, 1993b) study near the transition flow conditions of phase distribution. In the small-scale pipe, the phase distribution classifies into the wall-peak and the local void fraction increases with J_G where the shape of distribution remains to be almost similar one. On the contrary, the phase

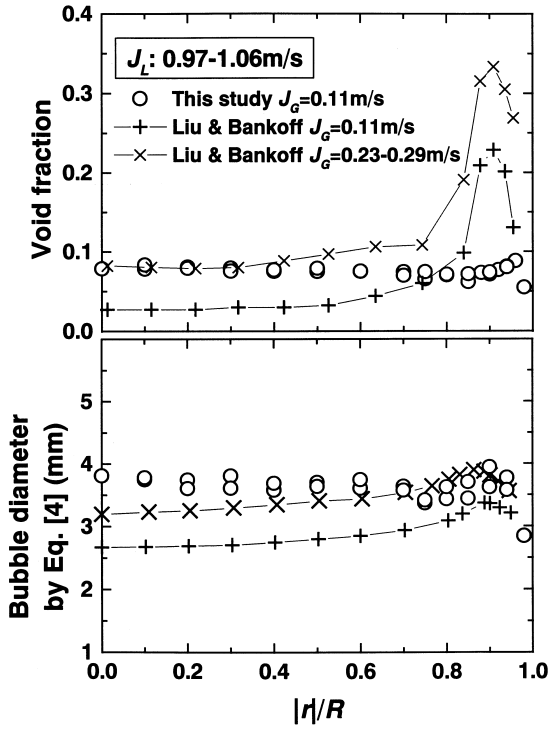

Fig. 14. Comparison of phase distribution and bubble diameter by Eq. (4) under wall-peak region with small-scale data.

distribution in this study is almost flat and the wall-peak is low. The bubble diameter in the small-scale pipe is lower in $|r|/R$ less than about 0.8 under the same J_G. The bubble diameter tends to be the same range under the higher J_G (0.23–0.29 m/s) for the small-scale pipe but the large difference for the height of wall-peak is still observed.

Many researchers have studied the prediction of the wall-peak phase distribution as a subject of numerical simulation (Anglart et al., 1993; Bertodano et al., 1994a,b; Minato et al., 1996). The wall-peak phase distribution could be simulated by assuming a lateral lift force, a turbulent dispersion force and so on under the framework of two-fluid model. Those constitutive equations depend on various physical quantities such as the bubble size, the velocity distribution and so on. The bubble size is almost the same range in Fig. 14 and the water and the bubble velocity distributions should be checked to make clear the reason giving the different height of wall-peak.

Fig. 15 compares the radial distributions of water velocity and its axial fluctuation at $L/D = 60$. The water velocity and the turbulent fluctuation under the single phase flow are almost the same regardless of the pipe scale except for the fluctuation near the wall. This indicates that the velocity gradient in the large-scale pipe is lower, and the lower gradient produces the lower fluctuation near the wall. Since the lift force model proposed by Drew and Lahey (1987) gives a larger lift force towards the wall under a higher velocity gradient, the lower velocity gradient is considered to be one of reasons that a high wall-peak is difficult to be maintained in the large-scale pipe.

Under the two-phase flow condition at $J_G = 0.11$ m/s, the lower velocity gradient is also realized although the value near the wall is slightly lower (maximum difference is about 0.2 m/s). However, the turbulent fluctuation is much higher than that in the small-scale pipe. Since the turbulent dispersion model proposed by Lahey and Bertodano (1991) depends on the liquid turbulent energy, the higher turbulent fluctuation produces a higher turbulent dispersion force. Since the higher turbulent dispersion force has a role to reduce the wall-peak value of void

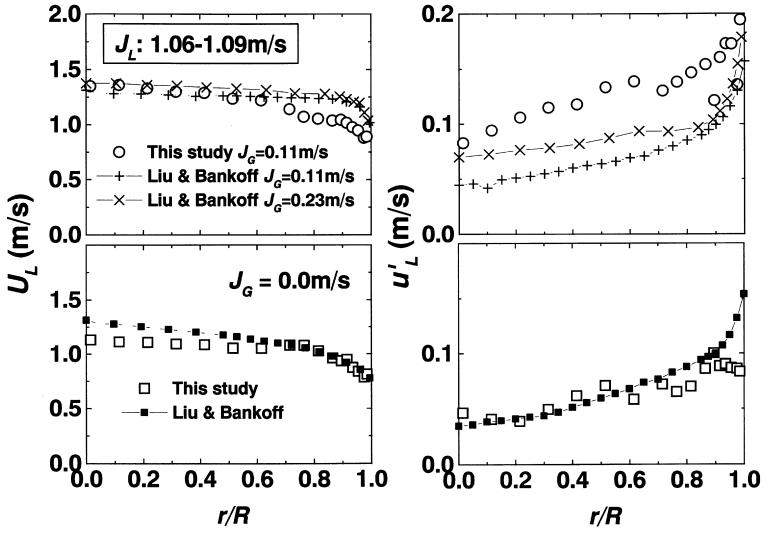

Fig. 15. Comparison of axial water velocity and velocity fluctuation with small-scale data.

fraction, the higher turbulent fluctuation is considered to cause the lower wall-peak in the large vertical pipe. In contrast, the higher turbulent fluctuation gives a higher liquid turbulent kinetic energy and a lower pressure field. The lower pressure field is considered to collect more bubbles near the wall and increase the wall-peak. This physical concept acts in the opposite to the turbulent dispersion force. We suppose that the effect of the pressure field has a smaller contribution against the velocity gradient and the turbulent dispersion. If the lower pressure field collects the bubbles, it is difficult to explain the lower wall-peak. Only the turbulent dispersion force can explain the lower wall-peak because the lower pressure field increases the wall-peak. We need to evaluate the contribution of the lower pressure field quantitatively in the future.

The bubble velocity and its turbulent fluctuation were almost the same regardless of the pipe scale. The bubble velocity affects the lift force through relative velocity based on the lift force model by Drew and Lahey (1987). No significant differences were recognized on the relative velocity between both pipes.

From the discussions up to here, the lower velocity gradient and the higher turbulent dispersion force are considered to cause the lower wall-peak in the large vertical pipe even under the same bubble size. The other factors affecting the transition of phase distribution are the bubble size and the formation of large eddies including bubble clusters under the agitated bubbly flow. The phase distribution was changed to a convex shape under the development of large coalescent bubbles as similar in small-scale pipes and the effect of bubble size itself is supposed not to depend on the pipe scale qualitatively. However, more comparisons are needed under various flow rates to quantify whether the threshold value of bubble size giving the transition depends on the pipe scale. This kind of quantitative discussion is a future subject, and detailed measurements to make clear the flow structure under the agitated bubbly flow have not been performed yet. The lower water velocity gradient and the higher turbulent fluctuation due to bubbles are supposed to contribute to the formation of agitated bubbly flow under a lower J_L. Detailed measurements under the lower J_L are also needed to make clear the scale effect in the future.

4. Concluding remarks

In order to investigate the dependency of gas–liquid two-phase flow on pipe scale, the transition characteristics of flow pattern and phase distribution were studied experimentally in upward air–water two-phase flow along a large vertical pipe (D: 0.2 m, L/D: 61.5). The experiments were conducted under the flow rate: 0.03 m/s $\leq J_G \leq$ 4.7 m/s (at top of test section), 0.06 m/s $\leq J_L \leq$ 1.06 m/s. Flow pattern was observed and measurements were performed on axial differential pressure, phase distribution, bubble size and bubble and water velocities. The scale effect on the phase distribution was discussed with small-scale data by Leung et al. (1995) and Liu and Bankoff (1993a,b).

As for the flow pattern, the flow conditions at which coalescence starts are almost the same as those found in small-scale pipes, but no large bubbles are observed in the region $L/D < 20$ which corresponds to the developing region of the axial differential pressure curves. The large coalescent bubbles were generated in $L/D > 20$. The churn flow is dominant in the large

vertical pipe under the conditions where small-scale pipes have slug flow. In contrast to small-scale pipes, the agitation of flow pattern is likely to be occurred under a lower J_L in the bubbly flow and under the flow pattern with large coalescent bubbles. Under the agitated bubbly flow, some large eddies including bubble clusters fill up the pipe. The flow direction of a cluster was random due to the large eddy and some bubble clusters with downward flow direction were frequently observed. In the churn slug/froth flow region, large coalescent bubbles flow intermittently as similar to the slug flow in a small-scale pipe but there are many small bubbles in the liquid film region between the large bubble and the wall.

The transition of phase distribution corresponds to the change of flow pattern. Large coalescent bubbles affect the phase distribution as similar to small-scale pipes but the core-peak phase distribution is established in the agitated bubbly flow under a low J_L where small-scale pipes have a wall-peak phase distribution. The large coalescent bubbles are developed along the test section via the churn bubbly flow where the phase distribution is a core peak one, whereas Taylor bubbles in small-scale pipes are generated at the vicinity of gas–liquid mixing region or are developed from the bubbly flow with a wall-peak phase distribution. The wall-peak in the large vertical pipe is lower even under the same bubble size. The lower peak is considered to be related to the lower radial velocity gradient of water and the larger turbulent dispersion force. More quantitative studies are needed for the scale effect on the contribution of liquid turbulent kinetic energy and on the threshold value of bubble size giving the transition from the wall-peak to the core-peak phase distribution. Detailed measurements are also needed to investigate the flow structure under the agitated bubbly flow.

Acknowledgements

The authors are profoundly grateful to Mr. M. Seimiya who performed the data processing work in this study.

References

Anglart, H., Andersson, S., Podowski, M.Z., Kunul, N., 1993. An analysis of multidimensional void distribution in two-phase flows. In: Proc. of the Sixth Int. Topical Meeting on Nucl. Reactor Thermal-Hydraulics (NURETH-6), Grenoble, 139–153.

Bataille, J., Lance, M., Marie, J.L., 1990. Bubbly turbulent shear flows. Advances in Gas–Liquid Flows FED-99 HTD-155, 1–7.

Bertodano, M.L., Lahey Jr., R.T., Jones, O.C., 1994a. Phase distribution in bubbly two-phase flow in vertical ducts. Int. J. Multiphase Flow 20 (5), 805–818.

Bertodano, M.L., Lahey Jr., R.T., Jones, O.C., 1994b. Development of a k–ε model for bubbly two-phase flow. J. Fluids Engineering 116, 128–134.

Drew, D.A., Lahey Jr., R.T., 1987. The virtual mass and lift force on a sphere in rotating and straining inviscid flow. Int. J. Multiphase Flow 13 (1), 113–121.

Dukler, A.E., Taitel, Y., 1986. Flow pattern transitions in gas–liquid systems: measurements and modeling. In: Hewitt, G.F., Delhaye, J.M., Zuber, N. (Eds.), Multiphase Science and Technology, vol. 2. Hemisphere, New York, pp. 1–94.

Hashemi, A., Kim, J.H., Sursock, J.P., 1986. Effect of diameter and geometry on two-phase flow regime and carry-over in a model PWR hot leg. In: Proc. of the Eighth Int. Heat Transfer Conf., San Francisco, CA, 2443–2451.

Hills, J.H., 1976. The operation of a bubble column at high throughput—I. Gas holdup measurements. The Chemical Engineering Journal 12, 89–99.

Kataoka, I., Ishii, M., 1987. Drift flux model for large diameter pipe and new correlation for pool void fraction. Int. J. Heat Mass Transfer 30 (9), 1927–1939.

Lahey Jr., R.T., Bertodano, M.L., 1991. The prediction of phase distribution using two-fluid models. In: ASME/JSME Thermal Eng. Proc., Reno Nevada, vol. 2, 193–200.

Leung, W.H., Eberle, C.S., Wu, Q., Ueno, T., Ishii, M., 1995. Quantitative characterizations of phasic structure developments by local measurement methods in two-phase flow. In: Proc. of the Second Int. Conf. on Multiphase Flow '95-Kyoto, IN2-17–IN2-25.

Liu, T.J., Bankoff, S.G., 1993a. Structure of air-water bubbly flow in a vertical pipe—I. Liquid mean velocity and turbulent measurements. Int. J. Heat Mass Transfer 36 (4), 1049–1060.

Liu, T.J., Bankoff, S.G., 1993b. Structure of air–water bubbly flow in a vertical pipe—II. Void fraction, bubble velocity and bubble size distribution. Int. J. Heat Mass Transfer 36 (4), 1061–1072.

Minato, A., Komatsu, I., Yamazaki, N., 1996. Numerical analysis of three-dimensional gas–liquid two-phase flow in subchannels of nuclear fuel assemblies. In: Proc. of the ASME Fluids Engineering Division Summer Meeting, San Diego, vol. 1, 75–80.

Mishima, K., Ishii, M., 1984. Flow regime transition criteria for upward two-phase flow in vertical tubes. Int. J. Heat Mass Transfer 27, 723–737.

Ohnuki, A., Akimoto, H., Sudo, Y., 1995. Flow pattern and its transition in gas–liquid two-phase flow along a large vertical pipe. In: Proc. of the Second Int. Conf. on Multiphase Flow '95-Kyoto, vol. 3, FT1-17–FT1-23.

Ohnuki, A., Akimoto, H., 1996. An experimental study on developing air–water two-phase flow along a large vertical pipe: effect of air injection method. Int. J. Multiphase Flow 22 (6), 1143–1154.

Ohnuki, A., Kamo, H., Akimoto, H., 1997. Developed flow pattern and phase distribution under gas–liquid two-phase flow in a large vertical pipe and prediction of phase distribution by multidimensional two-fluid model. In: Proc. of Eighth Int. Topical Meeting on Nucl. Reactor Thermal-Hydraulics (NURETH-8), Kyoto, vol. 3, 1670–1676.

Serizawa, A., Kataoka, I., 1988. Phase distribution in two-phase flow. In: Afgan, N.H. (Ed.), Transient Phenomena in Multiphase Flow. Hemisphere, New York, pp. 179–224.

Tomiyama, A., Sou, A., Zun, I., Kanami, N., Sakaguchi, T., 1995. Effects of Eötvös number and dimensionless liquid volumetric flux on lateral motion of a bubble in a laminar duct flow. In: Proc. of the Second Int. Conf. on Multiphase Flow '95-Kyoto, vol. 1, PD1-11–PD1-18.

Zun, I., Kljenak, I., Moze, S., 1993. Space-time evolution of the nonhomogeneous bubble distribution in upward flow. Int. J. Multiphase Flow 19 (1), 151–172.

Zun, I., Kljenak, M., Pecar, M., Polutnik, E., 1995. Bubble shape and interfacial area concentration measurements in upward and downward bubbly flow. In: Proc. of the Second Int. Conf. on Multiphase Flow '95-Kyoto, IN2-9–IN2-16.